Engineering Structures 354 (2026) 122396

Contents lists available at ScienceDirect

Engineering Structures

journal homepage: www.elsevier.com/locate/engstruct

Online PCCP wire break monitoring based on integrated and intelligent distributed fiber optic acoustic field sensing

Haoran Wang [a,d], Xuping Zhang [a,c,d], Imtiaz Naseeb Awan [a,d], Guangnan Zhou [a,d], Hongren Li [a,d], Jin Wang [g], Dao Zhang [f], Ningmu Zou [d,e,*], Yuanyuan Shan [b,**], Yixin Zhang [a,c,d,***]

[a] College of Engineering and Applied Sciences, Nanjing University, Nanjing 210023, China
[b] School of Physics and Optoelectronic Engineering, Nanjing University of Information Science & Technology, Nanjing 210044, China
[c] Shenzhen Research Institute of Nanjing University, Shenzhen 518000, China
[d] Key Laboratory of Intelligent Optical Sensing and Manipulation, Ministry of Education, Nanjing University, Nanjing 210093, China
[e] School of Integrated Circuits, Nanjing University, Suzhou 215163, China
[f] Nanjing Fiber Photonics Technology Co., Ltd, Nanjing 211135, China
[g] Beijing Shiyuan Technology Co., Ltd, Beijing 102400, China

ARTICLE INFO

Keywords:
Prestressed concrete cylinder pipe
Wire break
Distributed acoustic sensing
Health monitoring
Event locating

ABSTRACT

Prestressed Concrete Cylinder Pipe (PCCP) suffers from hidden and random wire breaks that severely affect the safety and service life of the pipe. The accumulation of such breaks can lead to pipe bursts, potentially causing heavy loss of life and property along the pipe. Traditional methods for identifying wire breaks require the pipe to be emptied for maintenance, and have limited ability to provide early warnings of wire break accidents during pipe operation. Therefore, monitoring of PCCP over the entire life cycle is essential for evaluating pipe health and preventing disastrous failures. In this paper, we have proposed an online PCCP wire break monitoring based on integrated and intelligent distributed fiber optic acoustic field sensing (I^2DAS). The system offers high localization accuracy and wide frequency response, ensuring that wire break events can be accurately targeted to individual pipe segments and the features can effectively reconstructed to distinguish them from environmental noise around the pipe. The system delivers a single-ended measurement range exceeding 20 km, supports a frequency response up to 50 kHz, and maintains an axial localization uncertainty of ±0.45 m. Laboratorial experiments as well as in-field experiments have proved the proposed method provides a reliable solution for online monitoring of PCCP wire break.

1. Introduction

Since the early 1940s, Prestressed Concrete Cylinder Pipe (PCCP) has been extensively utilized for water conveyance due to its high tolerance to overburden and working pressure, high-flow conveyance capacity, corrosion resistance, low operating costs, and excellent seepage control characteristics [1]. The technology has played a significant role in major water conservancy projects, such as the Arizona Center Project in North America, the Libyan Man-Made Great River Project in North Africa, and the South-to-North Water Diversion Project in People's Republic of China [2,3]. However, during the manufacturing, installation and operation of PCCP, the internal prestressed steel wires are susceptible to chemical corrosion or physical damage and consequent break [4]. Once the broken wires in a single section of pipe accumulate to a certain number, it can cause a sudden burst of the pipe, which not only stops the water, but also causes serious secondary disasters [5,6]. Therefore, there is a significant demand for real-time online monitoring of wire breaks over the entire service life.

Although traditional methods such as manual visual inspection and manual hammer inspection are widely used in long-distance applications, they are susceptible to subjective judgements and have significant limitations such as poor consistency, over-reliance on experience, and

* Corresponding author at: Key Laboratory of Intelligent Optical Sensing and Manipulation, Ministry of Education, Nanjing University, Nanjing 210093, China.
** Corresponding author.
*** Corresponding author at: College of Engineering and Applied Sciences, Nanjing University, Nanjing 210023, China.
E-mail addresses: nzou@nju.edu.cn (N. Zou), violetsyy@nuist.edu.cn (Y. Shan), zyixin@nju.edu.cn (Y. Zhang).

https://doi.org/10.1016/j.engstruct.2026.122396

Available online 25 February 2026

high labor consumption [7]. In order to solve these problems, electromagnetic detection [8], hydroacoustic monitoring [9], and distributed acoustic sensing (DAS) [10,11] have been introduced in recent years to perform monitoring of PCCP.

Electromagnetic detection method is based on the principle of remote field eddy current (RFEC). In 1958, T.R. Schmidt [12] developed the first RFEC detection system. In 2019, Xie [13] improved the wire break detection of PCCP based on the orthogonal electromagnetic principle and established detection system accordingly. However, due to the background noise caused by the conductivity change, the method has insufficient in detection accuracy and requires experienced operators to reduce false alarms [14]. Furthermore, electromagnetic detection method is only suitable for PCCP during the maintenance phase of water shutdowns during completion or major repairs. It cannot achieve online monitoring and its early warning capability for wire break-induced accidents during pipe operation is limited.

Since mid-1990s, hydroacoustic monitoring methods have been widely used commercially for PCCP wire break monitoring. In 2001, Mark Holley [15] successfully applied a hydrophone array to detect break signals on a 1.8 km section of PCCP in Maryland, USA. This method receives the wire break signals by installing point hydroacoustic sensors inside the pipe, and determines the location of breaks by calculating the difference in the arrival time of the break acoustic signals between two neighboring sensors. In 2010, G. Bell [16] used the hydroacoustic monitoring method to study the effect of PCCP wire breaks on the bearing capacity of the pipe, and distinguished phenomena such as wire breaks and mortar delamination through the amplitude and frequency response of the acoustic signal, thus evaluating the health status of the PCCP. In 2013, Elfergani [17] monitored the whole process of electrochemical corrosion using hydroacoustic emission technology for 14 days under laboratorial conditions, proving that the technology can identify wire breaks and early corrosion cracking of concrete. In 2016, Yao [18] developed a fiber-optic grating wire break monitoring system based on hydroacoustic, and the fiber grating vibration sensors installed on the inner wall of the pipe were able to achieve a wire break localization uncertainty of ±1.5 m and a frequency response range of 1 kHz. In 2019, Wei [19] used a low coherence fiber optic sensor (LCFS) to monitor the corrosion of a PCCP for a period of 6 months and found it to be an effective tool from early localized deterioration to eventual corrosion failure. The advantage of this method is that it is capable of continuous on-line monitoring without stopping the water supply and is highly resistant to interference. Hydroacoustic sensors typically need to be spaced less than 200 feet apart. Event location is based on the difference in arrival times of adjacent hydroacoustic sensors. However, differences in path length can lead to varying degrees of signal distortion, affecting localization and identification accuracy. In addition, the site installation, power supply, and communication of hydroacoustic sensors are complex, making it difficult to form networks over long distances, meanwhile the high installation cost limits the possibility of its wide application.

DAS uses fiber optics as the transmission and sensing element to provide non-contact acoustic measurement and multi-point monitoring, offering advantages in pipe safety monitoring. The continuously distributed sensing fibers can collect acoustic signals near the wire, providing unique advantages for PCCP wire break detection. Since 2006, M. S. Higgins [20] from Pure Technologies were pioneers in employing DAS for detecting wire breaks in PCCP. The technology was first used in the U.S.A. and successfully detected 11 breaks in four months, with a localization uncertainly of ±1.5 m. In 2022, Li [21] developed a PCCP break monitoring system, in which optical fibers are mounted on the inner and outer walls of a single section of the PCCP, and the signal over-zero rate and short-time energy of the signals are extracted to determine the wire break signals. In 2023, Ma [22] proposed an automatic monitoring method for PCCP wire break using DAS and used a deep learning algorithm to analysis the spectrogram of the signal.

Currently, there are limitations in monitoring PCCP wire breaks by relying solely on DAS technology, when the frequency of the vibration signal exceeds the frequency response of the DAS, the components higher than the frequency response are aliased as low frequency signals, resulting in an incomplete description of the high frequency characteristics of the wire break event, making it difficult to meet the requirements of monitoring and localization accuracy of the wire break event. In addition, existing methods require a large amount of data processing, suffer from environmental disturbances that affect event recognition, and lack the ability to build and iterate a template database, limiting their effectiveness.

From a system design perspective, these limitations stem from the inherent architectural trade-offs of conventional DAS. In these systems, the maximum vibration bandwidth that can be achieved is fundamentally coupled with the sensing range. This relationship is governed by the pulse repetition rate (PRR). Increasing the sensing distance requires reducing the PRR, which limits the detectable frequency range to the kilohertz level. Although high-frequency measurements can be realized over short distances using specialized interrogators, maintaining such high-bandwidth performance over long distances of tens of kilometers remains challenging.

This paper addresses the limitations of traditional wire break monitoring methods and proposes an integrated and intelligent distributed acoustic sensing (I^2DAS) specifically designed for PCCP wire break monitoring. The proposed system enhances the ability to perform long range and high frequency measurements. and location tests are performed on pipes to meet the monitoring requirements.

2. Origin of PCCP wire break

PCCP is composed of four main materials [23]: concrete, steel cylinder, prestressed steel wire and cement mortar, as shown in Fig. 1. The steel wire is wrapped around the outer layer of the steel cylinder and wind in a spiral with a tensile force to compress the cylinder and pipe core. It counteracts internal and external pressure and enhances the pipe structure. Due to the interaction between the manufactured materials and external environmental factors, damage to one material can initiate or accelerate damage to other materials, leading to break of the prestressing wires and the bursting of the PCCP.

As shown in Fig. 2, PCCP damage is a long-term process that can be divided into three main stages. In the early stage, newly manufactured pipes may have potential problems due to defects in the design, manufacturing, or installation process. In the medium stage, after installation and long-time service, these early failures, along with harsh external environments such as corrosion from environmental acids or erosion from pressurized water, can lead to cracking of the mortar protection layer. This cracking exposes the prestressing wires to harsh environment, resulting in wire break. In the late stage, cracks in the concrete of the pipe core and partial break of the prestressing wires can change the overall stress distribution of the pipe, generating pressures beyond the design capacity of the pipe, ultimately leading to leakage or even bursting of the PCCP.

In a late stage, cracks in the core concrete and partial breakage of the prestressing wires will change the overall stress distribution of the pipe,

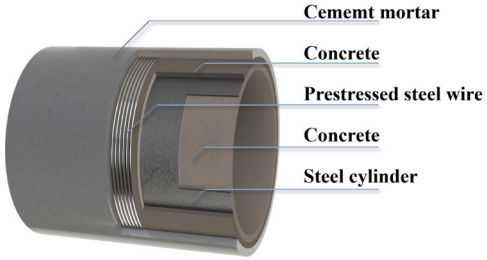

Fig. 1. PCCP structure.

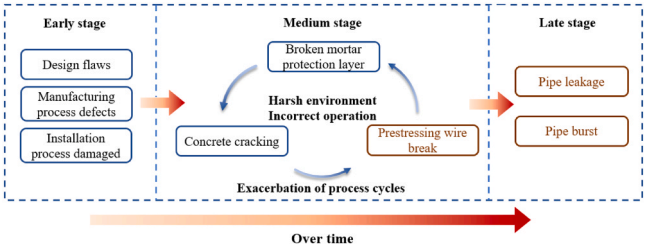

Fig. 2. PCCP damage process.

which will aggravate the occurrence of PCCP wire break in a short period of time, and the core concrete and steel cylinder will not be able to withstand the external loads and internal pressures, leading to bursting.

During the early stages of pipe deployment, risks associated with design, manufacturing, and installation can be mitigated through standardized operational procedures. However, once the pipe reaches the later stages, the accumulation of wire breaks can lead to structural damage, and the evolution of these breaks often results in rapid leaks or pipe bursts, making timely intervention difficult. Therefore, the mid-stage is crucial for online PCCP wire break monitoring. It is essential to continuously monitor the wire break status in each pipe section, assess the health of the pipe, and accurately determine the number and proportion of wire breaks in each segment. Early monitoring and prompt notification to the maintenance team can help prevent the progression to a later stage and avoid catastrophic pipe bursts.

Simultaneous break of multiple prestressing wires at the same location usually suggests that the pipe section has entered the terminal phase of the medium stage and is approaching the beginning of the late stage. At this point, the structural condition of the pipe is highly degraded and close to failure. Such a critical state does not occur abruptly. It is typically preceded by a sequence of progressively accelerating wire break events caused by stress redistribution and imbalance within the pipe structure. During this period, damage mechanisms such as concrete cracking and degradation of the mortar protection layer are intensified, leading to an exacerbation of the damage process cycle. As this process continues, the pipe rapidly evolves toward late stage failure modes, including pipe leakage and ultimately pipe burst.

3. I²DAS wire break monitoring system

3.1. integrated hardware structure

While DAS technology offers long-distance, meter-level spatial accuracy, its frequency response is typically limited by the sensing range, making it suitable mainly for monitoring vibrations below the kHz range [24]. In contrast, interferometric technology can detect frequencies up to the MHz range, but its spatial accuracy is relatively low, often only in the order of meters [7]. To address the challenges encountered in PCCP wire break monitoring, particularly with high-frequency vibration detection and precise spatial localization, a solution based on I²DAS technology is proposed. The optical schematic of the system is shown in Fig. 3.

The acoustic measurement unit of the system uses a continuous wave (CW) laser with a center wavelength of 1550.12 nm and a linewidth of 3.7 kHz as the light source. The light is split by a 50:50 coupler into a reference and a probe light. The probe light is modulated by an acousto-optic modulator (AOM) shift at a frequency of 40 MHz. The modulated signal amplified by an erbium-doped fiber amplifier (EDFA) and then injected into the sensing optical fiber by a wavelength division multiplexer (WDM). The optical signal passes through a bandpass filter (BPF) matched to the center wavelength, is reflected by a Faraday rotating mirror (FRM) and passes through a circulator into the coupler. The use of FRM at the end of the optical path automatically compensates for fiber

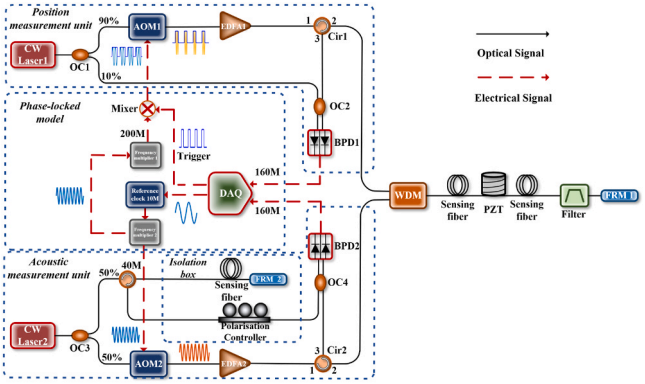

Fig. 3. Integrated monitoring system optical path diagram.

polarization state distortions and improves the stability of the signal.

The reference light is injected into the path corresponding to the length of the fiber after transmission through the circulator and is reflected by the FRM, the reflected light is adjusted by the PC and then passes back through the circulator into the 2 × 2 coupler, it interferes with the reference light and is finally detected by the BPD. During the detection process, the PC must be adjusted to ensure that the polarization states of the sensing light and the reference light are consistent, thereby improving the signal-to-noise ratio (SNR) of the IF signal and the accuracy of the signal demodulation. In addition, the reference part adopts a vibration isolation structure to effectively isolate external vibration and reduce environmental noise.

The location measurement unit of the system uses a CW laser with a center wavelength of 1561.40 nm and a linewidth of 3.7 kHz as the light source. The detected light is split into a reference light and a probe light using a 90:10 coupler. The probe light is then modulated by an AOM shift at 200 MHz to produce pulsed light. The pulsed light is further amplified by an EDFA and injected into the sensing fiber by a WDM. Since a 1560.00 nm bandpass filter is connected to the end of the sensing fiber, the sensing light cannot pass through the filter to reach the Faraday rotating mirror at the end, preventing the effect of the Fresnel reflection at the end of the fiber on the signal analysis of the location sensing unit. The backward Rayleigh scattered light generated by the pulsed light in the link passes through the circulator and interferes with the reference light in the 2 × 2 coupler, detected by the BPD finally.

The system adopts a phase-locked model to achieve synchronization between the data acquisition card (DAQ) and the AOM. The system is equipped with a dual-channel DAQ to ensure that the relative time error between the system modules is controlled at the picosecond level. 10 MHz clock and trigger signals are output from the DAQ simultaneously, and the 10 MHz signal is first multiplied to generate 40 MHz, and then further multiplied to obtain 200 MHz. 40 MHz signals are input to the AOM2, which provides the acoustic measurement module with continuous frequency modulation. The 200 MHz trigger signal is input to AOM1 for obtaining excellent wave cutting performance, which converts CW light into pulses with a pulse width of 32 ns and a frequency of 2 kHz.

The system uses a specialized sampling frequency to reduce data processing time. When the sampling rate f_s meets a specific multiplicative relationship with the IF signal frequency f_c, as in Eq. 1, a simplified phase demodulation algorithm can be used to reduce the amount of IQ demodulation [25]. In the system, the DAQ sampling rate is 160 MSPS, 40 MHz is selected for the AOM in the acoustic measurement unit and 200 MHz in the location measurement unit, both of which are in accordance with the scale requirements. By implementing IQ demodulation at this specific sampling rate, the real time computational load of the system is significantly reduced to meet the requirements of engineering applications [26].

$$f_s = \frac{4f_C}{2k-1} \quad (1)$$

In the experiment, the fiber link is placed inside a soundproof box, and a sine wave signal with a frequency of 20 kHz is applied to the PZT at the end of the fiber. The vibration location corresponded precisely to the single-mode fiber located at a distance of 20330 m. Fig. 4 shows the spatial temporal maps of the vibration region, a vibration stripe was shown at location 20330 m with a frequency matching the applied signal, at the same time, the width of the vibration region was 5 m.

Based on the sensing principle of the acoustic sensing module, we are able to simultaneously capture the characteristics of interference signals. When a 20 kHz vibration signal is applied to the PZT, a time-domain interference signal is generated within a 3 ms interval, as shown in Fig. 5. The inset in Fig. 5 provides a detailed view of these interference signals, the corresponding 20 kHz frequency spectrum is demodulated directly using Fourier transform. Therefore, the proposed vibration sensing system successfully demodulates the 20 kHz vibration event occurring at a distance of 20 km on the optical fiber.

To further validate the reliability of the proposed vibration sensing system, a series of high frequency vibration tests were conducted in the frequency range of 5 kHz to 50 kHz with 5 kHz intervals. This frequency range was chosen based on its complete coverage of the typical frequency band of wire break events [27]. The spectrum of the vibration signals is shown in Fig. 6, where each curve corresponds to a specific applied frequency and shows a distinct peak at the corresponding frequency.

To assess consistency, we statistically analyzed the peak power at each frequency. The results show that the standard deviation was 0.019 dB and the difference between the maximum and minimum values was 0.061 dB [28]. These metrics indicate an extremely small inter-peak disparity and a highly linear, uniform system response, supporting non-significant attenuation and non-frequency dead-zone characteristics for vibrations of up to 50 kHz over a 20 km measurement range. This verifies the system's suitability for monitoring PCCP wire breaks.

In summary, vibration signals can be precisely localized based on the signal testing of the location measurement system. Meanwhile, the acoustic measurement system is able to capture the vibration signals. The experimental results further validate the effectiveness of the proposed scheme in detecting high-frequency vibration signals in system. In conclusion, the system has no frequency dead zone in the detectable frequency range up to 50 kHz and supports vibration measurements over a distance of at least 20 km.

3.2. *intelligent signal processing flow*

To enhance the location accuracy of the wire break monitoring system, optimize resource utilization at the computational center, reduce data processing time, and establish a feature database, this study has

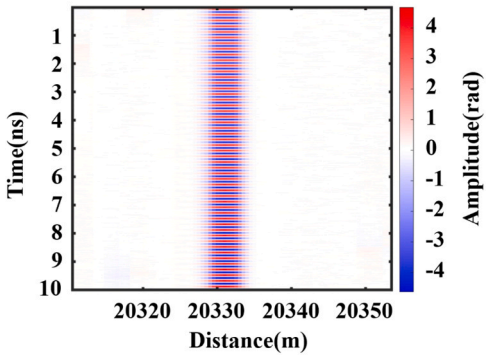

Fig. 4. Spatial temporal maps of the vibration region.

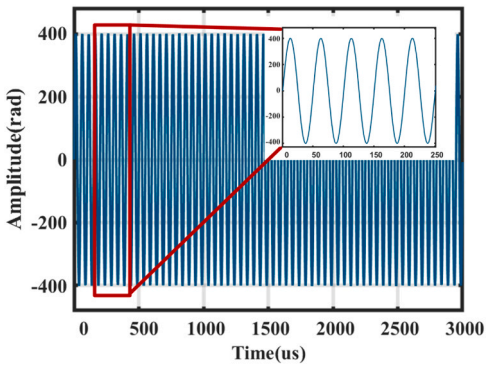

Fig. 5. Signal time-domain diagram.

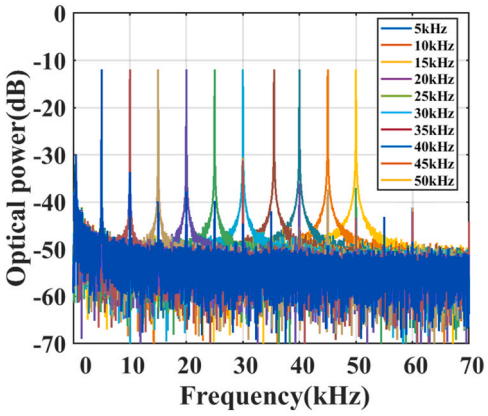

Fig. 6. Spectrum of vibration signal.

developed an intelligent data processing methodology, illustrated in Fig. 7. The approach consists of three interconnected modules: the acoustic sensing module, the location sensing module, and the feature matching module.

The acoustic sensing signals are first processed by the system. Although the proposed system demonstrates MHz-level vibration detection capabilities at the hardware and demodulation stages, the diagnostic information of PCCP wire break events is primarily concentrated within the sub-50 kHz spectrum. Consequently, to balance performance with computational efficiency, the demodulated acoustic signals are down-sampled to 100 kHz. This configuration ensures compliance with the Nyquist criterion for high-fidelity signal reconstruction while simultaneously mitigating data redundancy and processing latency, thereby optimizing overall system throughput.

The acoustic sensing module initiates with signal pre-processing to suppress environmental interference while preserving transient fault-related signatures. It is important to note that energy variation serves exclusively as an event-triggering mechanism rather than a definitive diagnostic indicator. Given that PCCP wire breaks generate impulsive and sporadic acoustic responses, short-time energy analysis is applied to detect abrupt signal changes and identify candidate analysis intervals. In this work, the window length is set to 100 ms to ensure effective capture of transient wire break signals.

In the feature matching module, the system matches test signals with stored acoustic fingerprints using feature synthesis techniques. A wire break is initially suspected upon detecting a sudden energy shift, but confirmation requires analyzing time-frequency characteristics against database references. Fast Fourier Transform (FFT) computes the spectrum of the time-domain signal $x[n]$. Each time slice is defined as $x_k[m]$. After segmenting the signal $x_k[m]$, a FFT is applied, which can be expressed as:

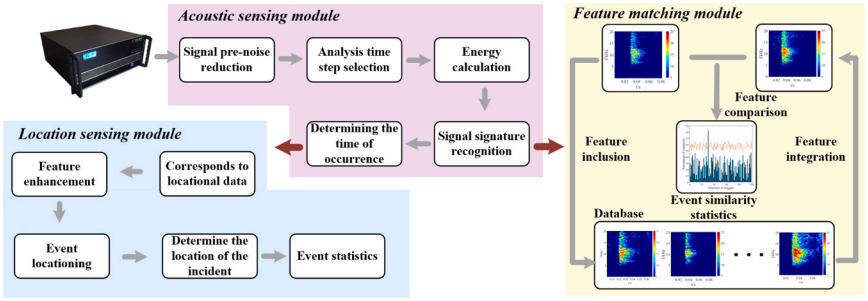

Fig. 7. Intelligent signal processing flow.

$$x_k[m] = x[k\cdot(L-overlap)+m], m = 0,1,\ldots,L-1$$
$$S(k,f) = \sum_{m=0}^{L-1} x_k[m]\cdot e^{-j2\pi fm/n_{fft}}, f = 0,1,\ldots,n_{fft}-1 \quad (2)$$

where x_k[m] is the result of slicing the k segment of the signal, where m is the index of the sample within the current segment and k is the index of the time segment. The signal is divided into overlapping segments. L denotes the length of each segment, and overlap is the number of overlapping samples between two adjacent segments. With segment length L set to 20 ms and overlap set to 25 %, the setup captures transient events effectively. Each segment undergoes an FFT. This results in a time-frequency matrix $S(k,f)$, which can be used to visualize the time-frequency distribution of the signal. The frequency band is divided into multiple sub-bands, and weights are applied based on the spectral characteristics of the wire break signal, allowing for tailored analysis and identification of key features $w(f)$.

$$w(f) = \begin{cases} w_1, f \in [f_1, f_2] \\ w_2, f \in [f_2, f_3] \\ \vdots \\ w_n, f \in [f_{n-1}, f_n] \end{cases} \quad (3)$$

$$S_i(k,f) = \sum_{i=1}^{n} w_i \sum_{f\in[f_{i-1},f_i]} |S(k,f)|^2 \quad (4)$$

After constructing a standard template for a single project, in order to realise the dynamic fusion of cross-project templates, we introduce a time decay mechanism and similarity weighting. Its time-frequency matrix is $S_m(k,f)$ appears at the generation time t_{n+1}, the new comparison template update formula is:

$$\lambda_{n+1} = e^{-\beta(t_{n+1}-t_n)}e^{-\alpha d_{n+1}}$$
$$S_m^{(n+1)}(k,f) = \frac{\lambda_{n+1}S_{n+1}(k,f) + (\sum_{i=1}^{n}\lambda_i)S_m^{(n)}(k,f)}{\lambda_{n+1} + \sum_{i=1}^{n}\lambda_i} \quad (5)$$

where λ_i denotes the weight of each event considering both time decay and template similarity, t_n is the generation time of the previous feature event, t_{n+1} is the current time, $\beta > 0$ is the time decay coefficient, d_{n+1} denotes the feature difference between the time-frequency matrix of new event and the current standard template, and $\alpha > 0$ is the similarity adjustment parameter.

Using this recursive updating mechanism, the system can adaptively construct a comparison template that reflects the latest signal features as it continuously generates new events. This improves the accuracy and robustness of the matching recognition. The extracted features are compared with those in the feature database using the Structural Similarity Index (SSIM) method. After calculating the similarity between the real and experimental values, a dynamic threshold is adjusted to identify the background noise. The statistical extraction of $S(k,f)$ represents the frequency points covered by the noise. From this, the mean and standard deviation of the noise can be computed. The formula is as follows:

$$\mu_n = \frac{1}{N_n}\sum_{f\in F_n}|S\left(k,f\right)|^2$$
$$\sigma_n = \sqrt{\frac{1}{N_n}\sum_{f\in F_n}\left(|S\left(k,f\right)|^2 - \mu_n\right)^2} \quad (6)$$

Where N_n represents the number of background noise frequency points, and F_n denotes the noise frequency range, which is typically selected from the low-frequency region with low energy as the noise bandwidth. To accommodate varying noise levels in different environments, the energy threshold is dynamically adjusted. The dynamic threshold T is defined as shown in the following formula:

$$T = T_B - \gamma\cdot\sigma_n \quad (7)$$

Where the dynamic threshold T is used to determine whether the signal to be detected differs significantly from the reference template, in order to identify abnormal events. T_B denotes the reference similarity threshold value, which is calculated from the threshold value obtained from the test as a threshold for the similarity before wire break. γ is a dynamic weighting factor that adjusts the threshold sensitivity to background fluctuations. The value can be set based on the actual noise level and the desired confidence interval. σ_n is the standard deviation of the background noise band. Representing the amplitude of similarity fluctuations, it is extracted and calculated from the low-frequency region or the noise stabilization band. This reflects the current level of environmental interference. The reference and test values are then compared. If the similarity exceeds threshold T, the event is categorized as an anomalous pipe break event and added to the database to generate feature templates.

In the location sensing module signals, the location data corresponding to the time points identified by the time sensing module is retrieved and processed. The location signals are then enhanced, and an angular point location method based on wave speed characteristics is applied to determine the location of significant events. DAQ supports dual-channel synchronous sampling with ps-level accuracy, eliminating the time offset between multiple independent systems. The acoustic propagation is represented in a time-distance image. The process begins with filtering by transforming the 2D location-time image, the zero-frequency component is shifted to the center of the frequency domain. 2D Fourier transform is applied, retaining only low frequency components near the center, allowing extraction of vibration contours is then restored to its original frequency arrangement, followed by an inverse 2D Fourier transform to reconstruct the spatial domain image. As shown in Fig. 8(a), the filtered image centers the fault event, with time delays forming slanting edges and energy gradually decaying outward. The time-domain representation exhibits a damped oscillation trend. After filtering, the features can be enhanced by detecting gray level discontinuities through gradient changes at different locations in the image. Let the grey value function of the image be I(x,y). At coordinates (x,y), a window w(u,v) is defined. As the window shifts by (Δx,Δy), the gray

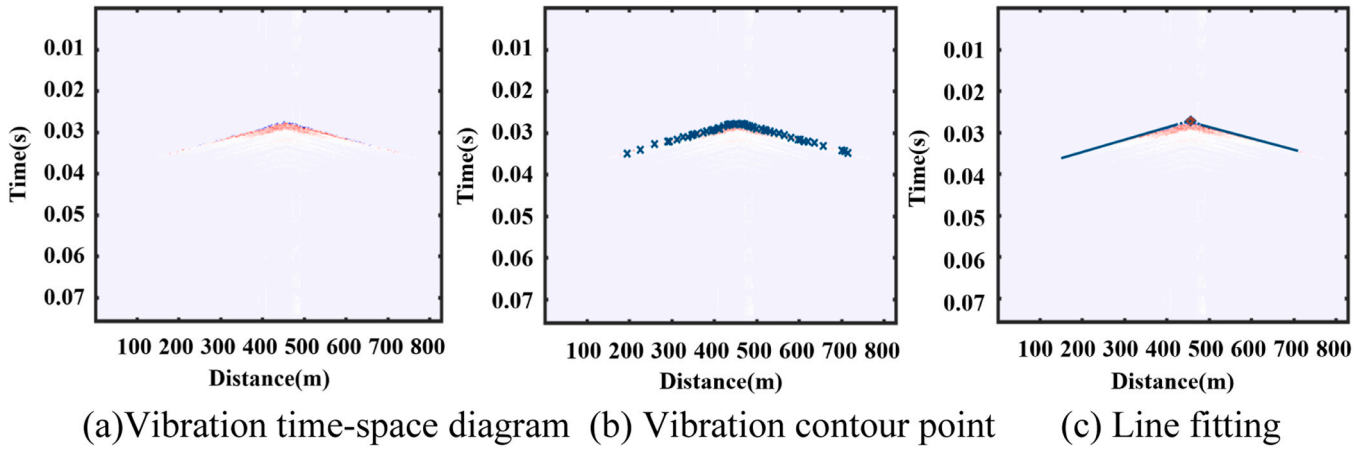

Fig. 8. Pipe event location.

level variation within the window, E(Δx,Δy), is defined as:

$$E\left(\Delta x,\Delta y\right)=\sum_{u,v}w\left(u,v\right)\left[I(x+u+\Delta x,y+v+\Delta y)-I(x+u,y+v)\right]^2 \tag{8}$$

Where I(x,y) represents the gray level of the image, w(u,v) is the window function, and Δx,Δy are the translation amounts of the window. Using a Taylor expansion to approximate the gray level variation:

$$E\left(\Delta x,\Delta y\right)\approx\left[\Delta x\quad\Delta y\right]M\begin{bmatrix}\Delta x\\ \Delta y\end{bmatrix} \tag{9}$$

In the formula, the matrix M represents a second-order matrix,

$$M=\sum_{u,v}w\left(u,v\right)\begin{bmatrix}I_x^2 & I_xI_y\\ I_xI_y & I_y^2\end{bmatrix} \tag{10}$$

The response function R is used to identify change points, as shown in the following equation:

$$\begin{aligned}R&=\det(M)-k\cdot trace^2(M)\\ \det(M)&=\lambda_1\lambda_2=I_x^2I_y^2-(I_xI_y)^2\\ \mathrm{trace}(M)&=\lambda_1+\lambda_2=I_x^2+I_y^2\end{aligned} \tag{11}$$

Where M represents the determinant of matrix M, trace (M) is the trace of M, and k is a scaling coefficient, with λ representing the eigenvalues of M, which indicate the extent of grayscale changes. When R, the response function derived from these parameters, exceeds a threshold, it can be interpreted as depicting the contour of the vibration waveform propagating from the source along the pipe. As shown in Fig. 8(b), the contour lines formed by these points exhibit a symmetrically centered distribution in space.

As shown in Fig. 8(c), after determining the contour points, the propagation direction of vibration in the pipe can be determined by linear fitting. Due to the complexity of the propagation and coupling relationship of the sound wave in the pipe, the coverage of the central region is discarded, and the contour points within the length of the pipe diameter are mainly used to conduct to the contour points on both sides of the pipe for linear fitting, so as to determine the center of the sound wave emitted.

$$m=\frac{N\sum_{i=1}^{N}x_iy_i-\sum_{i=1}^{N}x_i\sum_{i=1}^{N}y_i}{N\sum_{i=1}^{N}x_i^2-\left(\sum_{i=1}^{N}x_i\right)^2} \tag{12}$$

Based on the propagation speed of acoustic waves through the medium, using the concrete in the water pipe as the medium with a propagation speed of approximately 3000 m/s, the intersection of two calculated lines can be determined to pinpoint the axial location of the wire break.

$$m_{\min}\le m\le m_{\max} \tag{13}$$

By combining the frequency band characteristics of the acoustic signal with the acoustic wave propagation speed from the location recognition module for dual validation, the accuracy of the system is significantly improved. This method effectively mitigates the interference of external environmental noise, thereby improving the monitoring accuracy and efficiency. The integrated approach combines signal propagation speed, spatiotemporal features, and time-frequency characteristics, greatly improving the localization accuracy of break events. At the same time, it optimizes computational resources and reduces data processing time, providing a robust solution for distributed fiber optic sensing systems. For clarity and reproducibility, all symbols and variables used in this section are summarized in Table 1.

4. PCCP online monitoring experiment

4.1. setup of the monitoring experiment

To evaluate the ability of the integrated system to detect and locate wire breaks in PCCP, a simulated test was designed and conducted. The setup, as shown in the experimental setup diagram in Fig. 9, a total pipe length of 10 m, consisted of two pipes, sealed at both ends with welded steel plates.

Although the physical length of the PCCP section was only 10 m, the sensing cable bonded to the inner wall of the pipe was optically embedded within a continuous fiber link exceeding 20 km by introducing extension fibers on both sides. To verify the long-range sensing capability of the proposed I^{2}DAS system, a 20220 m extension fiber was connected between the interrogator and the upstream end of the sensing cable inside the PCCP, while an additional 200 m extension fiber was connected at the downstream end of the pipe and terminated by a FRM. In this configuration, the experiment effectively validates the single-ended sensing capability under a transmission distance exceeding 20 km.

The test environment is shown in Fig. 10(a). To ensure that the fiber optic cable enters the pipe smoothly and to keep the interface sealed and watertight, a special fiber optic cable entry assembly is installed at the bottom as shown in Fig. 10(b). In addition, venting value was installed the right of the pipe to displace the internal air, simulating full immersion of the pipe in actual operating conditions. The optical cable was attached to the inner wall of the pipe below using a polyurea coating,

Table 1
List of symbols and descriptions.

Symbol	Description
f_s	DAQ Sampling Rate
f_c	IF signal frequency
x[*n*]	Original time-domain signal
x_k[m]	The k-th segmented signal after time-domain segmentation
m	Sample index within the current segment
k	Time segment index
L	Length of each signal segment
S(k, f)	Time–frequency matrix obtained after transformation
w(f)	Sub-band weighting coefficients applied to wire break signal features
S_m(k, f)	Time–frequency matrix
t_{n+1}	Generation time of the current event
t_n	Generation time of the previous feature event
λ_i	Weighting factor combining temporal decay and template similarity
β	Time decay coefficient
d_{n+1}	Feature difference
α	Similarity adjustment parameter
N_n	Number of frequency points contained
F_n	Frequency band of background noise
T	Dynamic threshold
T_B	Reference similarity threshold
γ	Dynamic weighting factor
σ_n	Standard deviation of the background noise frequency band
I(x, y)	Gray-scale intensity value
w(u, v)	Window function
(Δx,Δy)	Displacement of the moving window
E(Δx,Δy)	Gray-level variation after window translation
M	Second-order matrix
R	Response function
k	Scaling coefficient
λ	Eigenvalues of matrix M

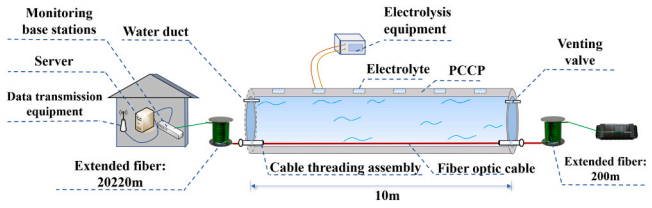

Fig. 9. Schematic layout of the wire break monitoring system.


(a) Test equipment


(b) Cable threading assembly


(c) Optical cable deployment

Fig. 10. Monitoring experimental physical map.

simulating the future installation method for real pipes as shown in Fig. 10(c). In this experiment, the internal water pressure of the PCCP was set to 0.4 MPa to accurately simulate the actual operating conditions. The resolution of the sensing system consists of two parts, the location measurement unit has a sampling rate of 2 kHz for each measurement point, with a spatial resolution of 3.2 m, and the acoustic measurement unit has an acoustic signal with a sampling rate of 100 kHz. According to the above division, the location processing unit can accurately determine the axial location of the wire break, and the acoustic processing unit with a high sampling rate ensures that the acoustic signals can be accurately captured and analyzed in detail.

The experiment has fully considered the effect of the acoustic wave propagation path on the signal attenuation as shown in Fig. 11, and the optical cable is laid according to the farthest acoustic wave path, the wire break event occurs at the top of the pipe, and the optical fiber is laid at the bottom. Although the fiber optic cable placed at the bottom of the pipe will cause attenuation of the acoustic wave during its propagation through the pipe, this method of placement represents the farthest path and verifies its effectiveness in detecting the breakage signal [29]. The advantage of distributed fiber optic sensing is that in the wire break event, the vibration will be sensed directly by the fiber optic along the closest path of pipe. Reliable monitoring even at the farthest path ensures that the fiber can be laid at any angle in the pipe to support effective monitoring. In this experiment, the vibration sensing optical cable used is φ-OTDR special optical cable, which is designed for long-distance vibration fiber optic sensing system. The core fiber type of the cable is G.652D standard single-mode fiber, the number of cores is 4, the diameter of the fiber is 0.25 mm, and the attenuation at 1550 nm wavelength is less than 0.30 dB/km. The optical cable structure adopts the center bundle tube design, the center is a PBT tube, filled with fiber optic special grease to provide waterproof and buffer protection, the external reinforcement element consists of 8 stranded galvanized steel wires with a diameter of 1.2 mm armored for mechanical protection, the outermost layer is a HDPE sheath, and the overall cable outside diameter is 7.0 mm. This structure gives the cable high vibration susceptibility and mechanical strength, and it is suitable for the internal laying of pipes.

The PCCP had an internal diameter of 3.2 m and the prestressed steel wires were 7 mm in diameter. The thickness of the mortar protective layer was 32 mm, and the external concrete layer had a thickness of 198.5 mm. A total of 20430 m of fiber is connected to the equipment, of which 20220 m of extension fiber is connected between the equipment and the pipe under test to meet the design requirements. The experiment involved digging grooves in the outer layer of the pipe to expose the prestressed steel wires, as shown in Fig. 12(a). The corrosion process of the steel wires was accelerated using electrochemical methods to test the ability of the system to accurately detect strand wire breaks within the distance of a single pipe shown in Fig. 12(b). This approach serves as a reference for future pipe maintenance decisions.

4.2. detection and localization of wire break event

The experiment began by activating the equipment and applying an electric current to the electrolytic solution inside the grooves. The DC voltage was set to 24 V and the current to 4 A in order to accelerate the dissolution of the steel wire. During the monitoring phase, the energy of

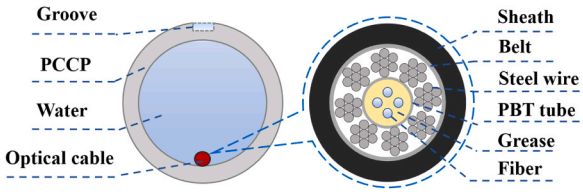

Fig. 11. Optical cable location and structure in the pipe cross section.

(a) Detail of pipe after trenching (b) Detail of break after corrosion

Fig. 12. Electrolytic corrosion diagram.

the real-time signals generated by the acoustic sensing module was initially filtered. As shown in Fig. 13, the energy statistics over a single test period reveal a sudden increase in the energy level of the pipe, followed by a rapid decrease as the noise level returns to a stable state. This indicates the occurrence of an abnormal event in the pipe.

Six distinct time intervals were extracted from the data presented in Fig. 13. Using Eq. 2, we conducted a detailed analysis of the segmented signals and applied a time-frequency signal analysis method. This method effectively removed both environmental and human-induced interference, specifically targeting pipe wire break events. During the analysis, the window length was set to 1000 samples, with an overlap of 250 samples. For frequency band weighting, interference below 3 kHz was filtered out, while equal weighting was applied to the frequency range of 3 kHz to 50 kHz. The time-domain waveforms and time-frequency spectrum are presented in Fig. 14, organized according to the sequence of trigger times.

After passing the time-frequency images into the database for comparison, the similarity statistics can be obtained as shown in Fig. 15. The initial threshold was determined using a confidence interval-based optimization method to ensure the statistical reliability of the screening process. Specifically, it was first assumed that the similarity of the break wire events obeyed an approximate normal distribution, and the sample mean of the group was 88.62 %, and its standard error was 2.76 %. For the 99 % confidence level, the lower threshold of the confidence interval was calculated as 80.34 %. Events 1 and 3 with similarity values below this threshold were screened out, while similarity values above the threshold were retained. This approach provides high statistical confidence by quantifying the estimated uncertainty of the sample mean and effectively avoids the effect of low similarity environmental disturbance events.

Four wire break events were successfully identified, matching the actual number of breaks in the pipe, thereby validating the accuracy of the data processing method. The remaining two events are the test site environment. The acoustic sensing module and the feature generation effectively met the requirements for detecting the acoustic signals associated with wire break events. Feature analysis of the four break events revealed that their durations ranged from 10 ms to 20 ms. The time-domain signals peaked approximately 5 ms after the event onset, gradually decaying to normal levels. The peak-to-peak value of the signal was approximately 205 rad. As shown in Fig. 16, the vibration frequency peaked at 28 kHz, with resonance peaks occurring around 12 kHz and 18 kHz, lasting for about 10 ms. Subsequently, the low-frequency energy below 13 kHz gradually decayed, completely dissipating after 10 ms. This pattern reflects the instantaneous energy release during the metal break, triggering a continuous resonance effect. In contrast, the signal duration for environmental or human-induced noise events was much longer, indicating a clear distinction between the break events and non-break disturbances. The signal duration for environmental or human-induced noise event 1 was 24.5 ms, with a peak frequency of only 12 kHz, which was significantly longer than that of the wire break events and did not match the characteristics of the break signals. Event 3, on the other hand, had a signal duration of only 3.5 ms, with the main frequency band concentrated between 5 kHz and 10 kHz, which also did not align with the break signal characteristics.

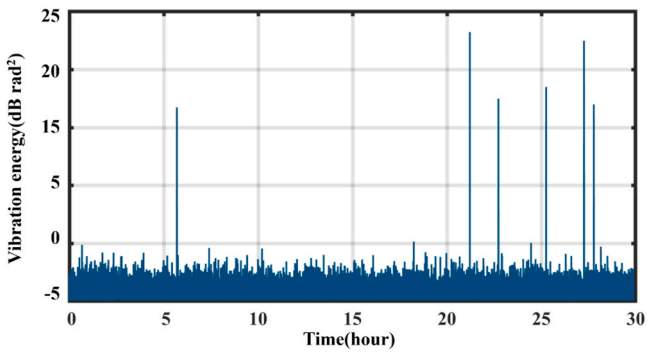

Fig. 13. Pipe energy statistics.

In practical PCCP monitoring scenarios, wire break detection is formulated as an anomaly identification problem. However, it should be noted that not all energy variations observed by the sensing system correspond to wire breaks. Various non-target events may also introduce energy fluctuations in the acoustic signals [15]. According to their physical origins and signal characteristics, potential energy-varying events can be classified into four categories: (1) Hydraulic-related events, including pump start/stop operations, valve adjustments, pressure transients, and water hammer effects; (2) Environmental and external disturbances, such as ground-borne vibrations induced by nearby traffic or construction activities. In large-diameter PCCP systems deployed along highways, heavy vehicles may generate sustained low-frequency broadband vibrations, typically concentrated below 50 Hz [30]; (3) Operational or human-induced activities, including maintenance operations, equipment handling, and accidental impacts; (4) System-intrinsic artifacts, such as laser phase noise, polarization fluctuations, and electronic noise [31]. Although these events may cause noticeable energy variations, they differ fundamentally from wire break events in terms of signal duration, dominant frequency band, and spatial characteristics. Wire break events are typically characterized by short-duration impulsive responses, high-frequency components in the kHz range, and localized spatial signatures. These distinctions form the physical basis for the subsequent intelligent signal processing and similarity-based classification.

The frequency of template event with a selected time window length of 10 ms were statistically analyzed, and the results are shown in Fig. 17.

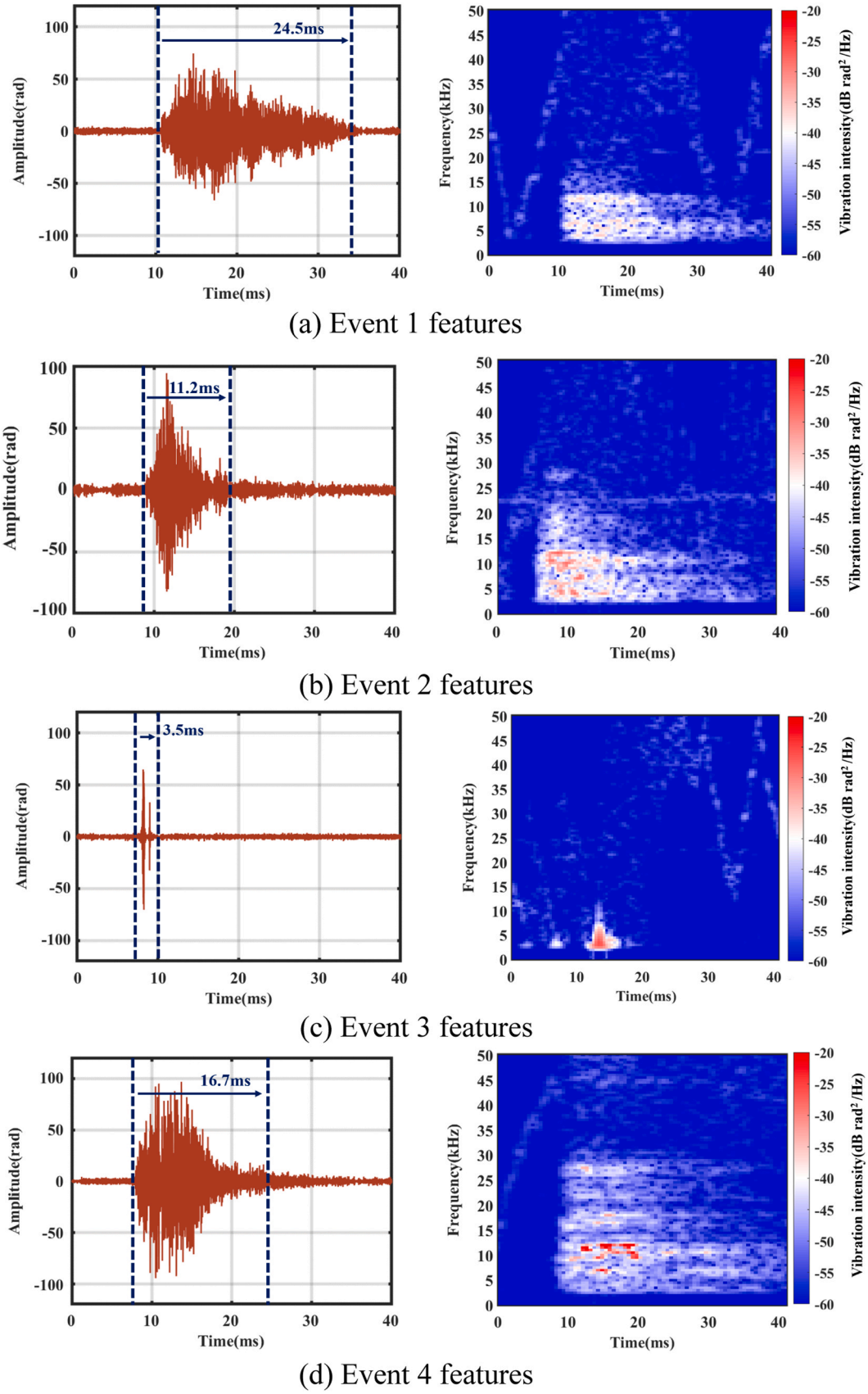

Fig. 14. Abnormal events time domain diagram and time frequency diagram.

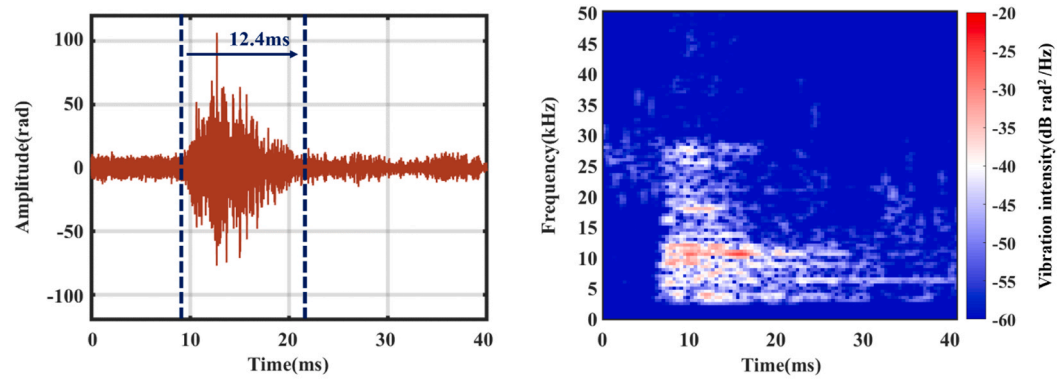

(e) Event 5 features

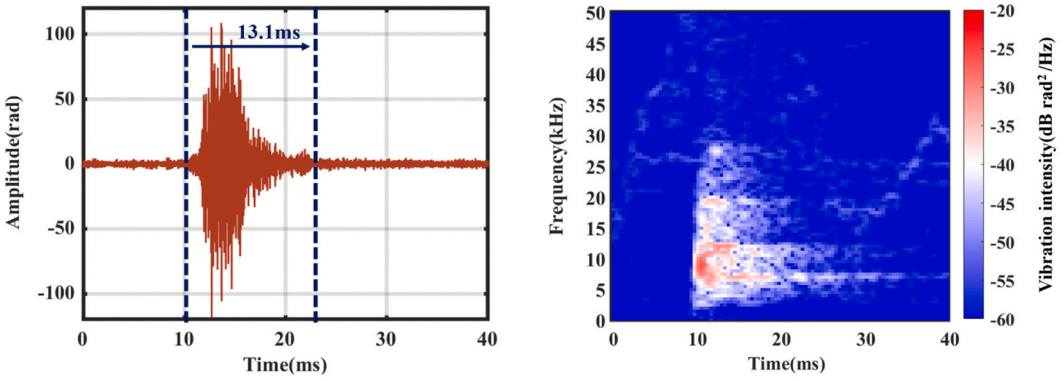

(f) Event 6 features

Fig. 14. (*continued*).

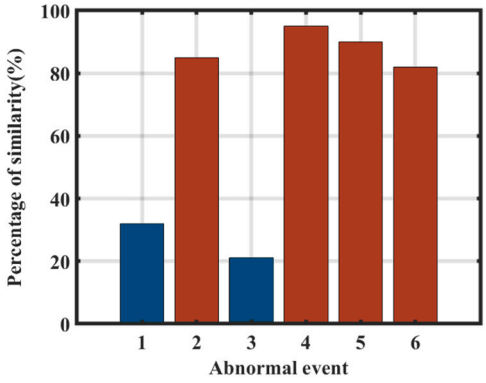

Fig. 15. Similarity of anomalous events.

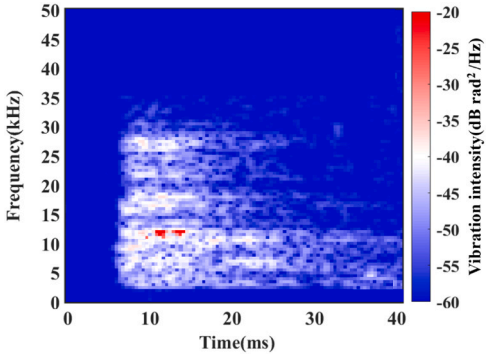

Fig. 16. Wire break event template.

The signal exhibited distinct peaks in the frequency domain, indicating that the system is capable of accurately identifying the characteristic resonance points during the vibration process, thus effectively distinguishing between different events. To improve the accuracy of event recognition, we filtered the selected frequency bands and increased the weight coefficients within these bands, significantly enhancing the recognition accuracy.

As an example of a wire break event, we analyzed the data from the location sensing module based on the trigger time of the event. In Fig. 18 (a), the spatiotemporal global map is shown, where different colors represent the energy intensity detected at various locations over time. This map includes data collected within 10 s of the event trigger, with red highlights clearly indicating the exact time and axial location of the break event. After confirming the break event with the acoustic sensing module, we extracted the data within 1 s after the trigger point for a detailed analysis. The zoomed view in Fig. 18(b) illustrates how the energy sharply rises to a peak at the moment of the break, followed by a gradual decay. The energy distribution in space appears symmetrical, radiating outward from the break location. The energy forms a slanting pattern according to the time delay effect of the acoustic wave and weakens progressively with the increasing distance from the break point.

Contour point location method based on wave speed characteristics to accurately determine the axial location of events. By monitoring the contour patterns, these contour points were then fitted with a straight line, allowing for the calculation of the acoustic wave propagation speed and verification of the acoustic source location accuracy. The intersection of the fitted lines offered the accurate axial location along the fiber, with the calculated location at 20228.5 m, within the predefined pit range.

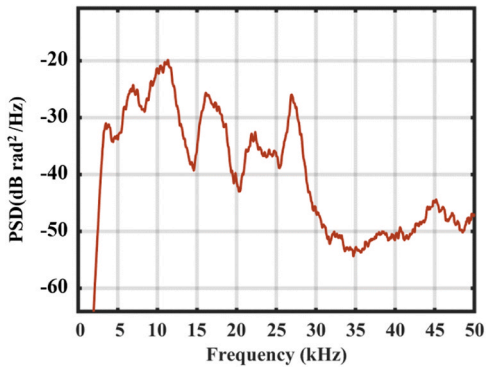

Fig. 17. Wire break event signal spectrum.

To verify the repeatability of the results, A total of four corrosion pits on the pipe were tested, with four wire break signals generated in each pit. The test results showed that the localization error for the vibration events was controlled within ±0.45 m as shown in Fig. 19(a). The conventional method uses an energy integration method, which integrates the statistics along the time axis for the region of instantaneous energy increase and extracts the peak at the center from the local energy distribution as the axial location of the wire break [32]. This method achieves a localization uncertainty of ±1.31 m as shown in Fig. 19 (b). In comparison, the localization uncertainty of the method in this paper is about 65.6 % improvement in localization accuracy. This data confirms the reliability and stability of the integrated distributed fiber optic sensing system in break event detection and localization.

To assess the correlation between wire breakage events and the corrosion process, this study statistically analysed six sets of experimental data simultaneously. Each set of data recorded the time series from the onset of corrosion to four consecutive wire break events occurring, as shown in Fig. 20. The results showed that the first wire break event times ranged from 18.6 to 24.1 h according to the corrosion rate. The mean intervals were calculated by summarising the events in order as 2.525, 1.298 and 0.548, with respective standard deviations of 1.083, 0.559 and 0.276. These intervals showed a decreasing trend with high variability in the early stage, reflecting the significant effect of initial corrosion conditions on event timing.

Pearson's correlation coefficient analysis based on the 18 interval data showed a medium-strength negative correlation between event order and interval time with a correlation coefficient of −0.757 and a p value of 0.000278. The slope of the linear regression was approximately −0.938, indicating that each additional event order resulted in a significantly shorter interval time. This negative correlation supports the hypothesis of a cumulative effect of corrosion, where the initial accumulation of damage takes a longer time and may be accelerated by later damage due to stress imbalances in the structure.

In addition, the mean value of total wire break time for each group was 4.373 h. Comparisons between groups showed that the first group had the longest total duration of 6.58 h and the most widely spaced intervals, while the fourth group experienced the shortest duration of 3.01 h and the most dense events. The first interval was longer in most groups, with subsequent intervals gradually decreasing. This indicates that events occurred more slowly in the early stages of corrosion and tended to be denser in the later stages.

This accelerating pattern suggests that catastrophic failure is not the result of a sudden and isolated simultaneous collapse of multiple wires, but rather the culmination of a progressive damage process

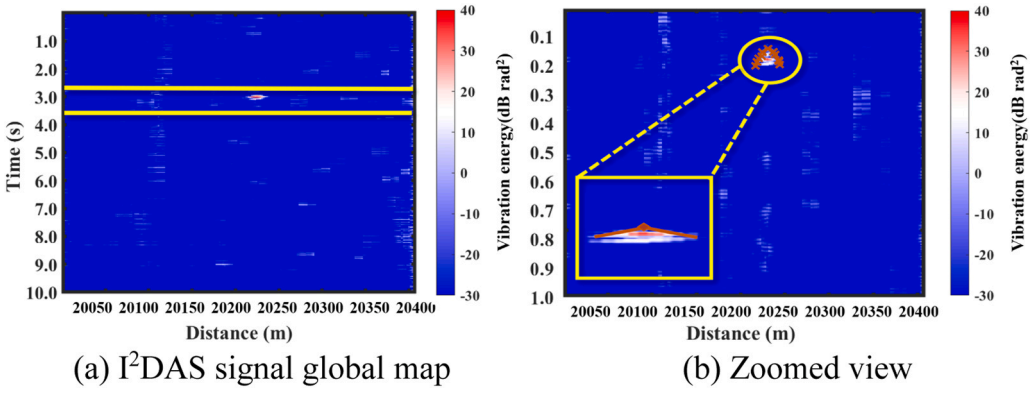

Fig. 18. Axial localization results of the location sensing module.

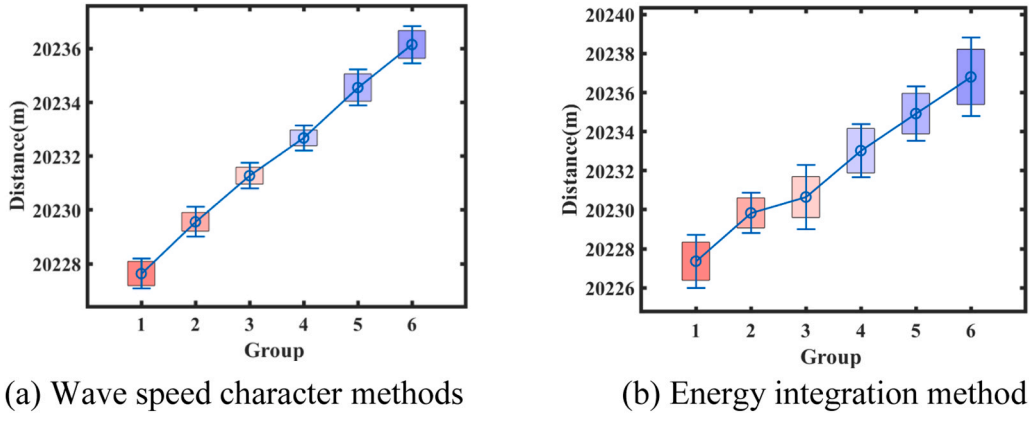

Fig. 19. Axial localization comparison.

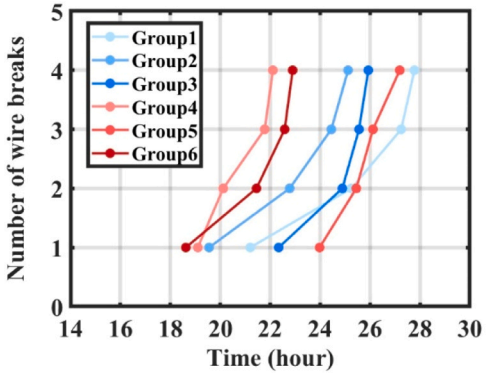

Fig. 20. Wire break time series during corrosion.

characterized by increasingly frequent wire breaks. In cases where multiple prestressing wires appear to break at nearly the same location and time, such behavior can be interpreted as the final manifestation of this acceleration process, occurring when stress redistribution and imbalance have reached a critical level within the pipe structure. Therefore, closely spaced or near-simultaneous wire breaks indicate an advanced stage of structural deterioration. The acceleration trend quantified in this study provides a quantitative basis for assessing corrosion risk. In future work, this trend can be further captured using decay or acceleration models to improve predictive accuracy.

5. Conclusion

This study presents a novel method for monitoring PCCP wire breaks based on an integrated distributed optical fiber acoustic sensing approach. The method combines phase rapid demodulation processing technology at special sampling rates, which not only meets the monitoring performance requirements but also significantly enhances computational efficiency. During the signal post-processing phase, we integrate spatiotemporal features, time-frequency characteristics, and wave velocity features, greatly improving the accuracy of wire break event localization and reducing data processing time. This offered an efficient solution for PCCP wire break monitoring. Additionally, through field trials, we conducted real-world analysis of the characteristic frequency bands and specific locations of acoustic signals generated by wire break events. The results demonstrate that the system can accurately capture PCCP wire break events during pipe operation. The system achieves a measurement range of over 20 km with a frequency response of up to 50 kHz, while the axial localization error is maintained within ±0.45 m, a 65.6 % improvement in accuracy over energy integration methods. These performance metrics meet wire break monitoring standards and highlight the effectiveness of the method in pipe health monitoring.

CRediT authorship contribution statement

Yixin Zhang: Supervision, Funding acquisition, Conceptualization. **Yuanyuan Shan:** Supervision, Funding acquisition, Conceptualization. **Ningmu Zou:** Supervision, Funding acquisition, Conceptualization. **Imtiaz Naseeb Awan:** Formal analysis. **Xuping Zhang:** Supervision, Funding acquisition, Conceptualization. **Haoran Wang:** Writing – review & editing, Methodology. **Dao Zhang:** Software, Formal analysis. **Jin Wang:** Funding acquisition. **Hongren Li:** Data curation. **Guangnan Zhou:** Writing – original draft.

Declaration of Competing Interest

The authors declare that they have no known competing financial interests or personal relationships that could have appeared to influence the work reported in this paper.

Acknowledgements

This work was supported by National Natural Science Foundation of China (NSFC) under Grant (62175100), and Fundamental Research Funds for the Central Universities (2024300447).

Data availability

Data will be made available on request.

References

[1] Kenny Michael K, Rahman Shah. "San diego county water authority aqueduct protection program since 1992: evolution in design and construction of steel cylinder relining of PCCP. Pipelines 2014 Undergr Forefr Innov Sustain 2014: 872–86.
[2] Williams, Bethany A, Ron LAblin, Brandy AKelso. PCCP inspection: prioritizing risk, assessing shutdown impacts, and executing the inspection. Pipelines 2007 Adv Exp Trench Pipeline Proj 2007:1–9.
[3] Kuwairi A. Water mining: the great man-made river, Libya[C]. Proceedings of the Institution of Civil Engineers-Civil Engineering, 159. Thomas Telford Ltd; 2006. p. 39–43.
[4] Zhao XF, Zhang J, Yuan HY. Considerations of enhancing project safety of PCCP water conveyance[J]. China Water Resour 2021;8:42–5.
[5] Rizzo P, et al. Water and wastewater pipe nondestructive evaluation and health monitoring: A review. Adv Civ Eng 2010;2010.
[6] Liu Z, Kleiner Y. State of the art review of inspection technologies for condition assessment of water pipes. Measurement 2013;46:1–15.
[7] Xuping Z, Guangnan Z, Haoran W, et al. Research progress of broken wire monitoring of pccp pipeline based on distributed optical fiber acoustic sensing. Acta Opt Sin 2024;44:149–60.
[8] Xiaojie X, Zhanbin Z, Yueling J. Research on e-shape magnetic core based self-differential mode pick-up coil and its application for fine crack non-destructive testing. AASRI International Conference on Industrial Electronics and Applications. Atlantis Press; 2015. p. 76–80.
[9] Tianxiang L, Shaokong F, Guanlin Y. Tests for leakage monitoring method of large pressure water pipeline. J Vib Shock 2021;40:136–42.
[10] Huang J, Zhou Z, Zhang D, Wei Q. A fiber bragg grating pressure sensor and its application to pipeline leakage detection. Adv Mech Eng 2013;5:590451.
[11] Huang J, Zhou Z, Zhang D, et al. Online monitoring of wire breaks in prestressed concrete cylinder pipe utilising fibre bragg grating sensors. Measurement 2016;79: 112–8.
[12] Schmidt T. History of the remote-field eddy current inspection technique: Materials evaluation, vol. 47, no. 1, pp. 14–22 (jan. 1989). NDT Int 1990;23(364).
[13] Xie Y, Feng H, Zhao M, Zeng Z. Pccp broken wire detection based on orthogonal electromagnetic principle. J Meas Sci Instrum 2019.
[14] Kaixu G, Yuan G, Xiguo L. Discussion on PCCP safety performance and wire breakage detection technology. Technol Sci Innov 2020;3:104–6.
[15] Holley M, Diaz R, Giovanniello M. Acoustic monitoring of prestressed concrete cylinder pipe: A case history. Pipelines 2001 Adv Pipelines Eng Constr 2001:1–9.
[16] Bell G.E., Paulson P."Measurement and analysis of pccp wire breaks, slips, and delaminations," in Pipelines 2010: Climbing New Peaks to Infrastructure Reliability: Renew, Rehab, and Reinvest, (2010), pp. 1016–1024.
[17] Elfergani HA, Pullin R, Holford KM. Damage assessment of corrosion in prestressed concrete by acoustic emission. Constr Build Mater 2013;40:925–33.
[18] Xuande Y. Beijing south-to-north water diversion project pccp pipeline wire breaking and leakage real-time monitoring integrated system. Water Conserv Hydropower Technol 2016;47:67–72.
[19] Wei H, Liao K, Zhao X, et al. Low-coherent fiber-optic interferometry for in situ monitoring the corrosion-induced expansion of pre-stressed concrete cylinder pipes. Struct Health Monit 2019;18:1862–73.
[20] Higgins MS, Paulson PO. Fiber optic sensors for acoustic monitoring of pccp. Pipelines 2006 Serv Own 2006:1–8.
[21] Li Y, Sun K, Si Z, et al. Monitoring and identification of wire breaks in prestressed concrete cylinder pipe based on distributed fiber optic acoustic sensing. J Civ Struct Health Monit 2022;14:3–14.
[22] Ma B, Gao R, Zhang J, Zhu X. A yolox-based automatic monitoring approach of broken wires in prestressed concrete cylinder pipe using fiber-optic distributed acoustic sensors. Sensors 2023;23:2090.
[23] Xu W, Ye Y, Lei W. Experimental study on identifying the number of wire breaks in prestressed concrete cylinder pipe based on piezoelectric sensing technology. Constr Build Mater 2024;422:135762.
[24] Xiong F, Qu BY, Zhou GN, et al. A broken wire detection system of PCCP pipeline based on Φ-OTDR and MZI[J]. Optoelectron Technol 2023;43(02):133–41.
[25] Zhang C, Zou NM, Song JY, et al. Digital signal processing and application of Φ-OTDR system[J]. OptoElectron Eng 2023;50(2):220088.
[26] Zabihi M, Chen Y, Zhou T, et al. Continuous fading suppression method for Φ-OTDR systems using optimum tracking over multiple probe frequencies. J Light Technol 2019;37(14):3602–10.

[27] Fei X, Boyang Q, Guangnan Z, et al. A PCCP filament breakage monitoring system integrating Φ-OTDR and MZI. Optoelectron Technol 2023;43(02):133–41.
[28] Sun Zhenshi, et al. Distributed vibration sensing with high frequency response by using WDM based integrated scheme. J Phys D Appl Phys 2020;53(15):155106.
[29] Leinov Eli, Lowe Michael JS, Cawley Peter. Investigation of guided wave propagation and attenuation in pipe buried in sand. J Sound Vib 2015;347:96–114.
[30] Shao Jie, et al. Near-surface characterization using urban traffic noise recorded by fiber-optic distributed acoustic sensing. Front Earth Sci 2022;10:943424.
[31] Shang Ying, et al. Research progress in distributed acoustic sensing techniques. Sensors 2022;22(16):6060.
[32] Xuping Z, et al. Performance optimization for a phase-sensitive optical time-domain reflectometry based on multiscale matched filtering. Opt Eng 2019;58:5.